

Article

Vertical Divergence Characteristics of Dissolved Inorganic Carbon and Influencing Factors in a Karst Deep-Water Reservoir, Southwest China

Zhongfa Zhou ^{1,2,3}, Cui Wang ^{2,3,*}, Yongliu Li ^{1,3}, Yongrong Zhang ¹ and Jie Kong ^{2,3}

¹ School of Karst Science, Guizhou Normal University, Guiyang 550001, China; fa6897@gznu.edu.cn (Z.Z.); 19010170428@gznu.edu.cn (Y.L.); 17030170026@gznu.edu.cn (Y.Z.)

² State Key Laboratory Incubation Base for Karst Mountain Ecology Environment of Guizhou Province, Guiyang 550001, China; 223100170049@gznu.edu.cn

³ School of Geography and Environment, Guizhou Normal University, Guiyang 550001, China

* Correspondence: 201609006@gznu.edu.cn; Tel./Fax: +86-0851-83222932

Abstract: In deep karst reservoirs, the internal environment is complex, and thermal stratification is not the only factor controlling the vertical distribution of the DIC concentration. Previous studies have not fully understood the migration and transformation of DIC in a deep-water reservoir. In this study, a deep-water reservoir in southwest China was chosen, and the spatial and temporal characteristics of the DIC concentration, pCO₂, δ¹³C_{DIC} value, and Sic were investigated. It was found that the Pingzhai Reservoir is a double temperature leapfrog reservoir. The DIC concentration, pCO₂, Sic, and δ¹³C_{DIC} values showed annual cycle variation. During the thermal stratification phase, the DIC concentration, pCO₂, Sic, and δ¹³C_{DIC} values were significantly different between the surface layer and the lower layer. However, during the mixing and mixed phases, the differences were not significant. The vertical divergence of the DIC in the Pingzhai Reservoir was influenced by the subtemperate layer, human activities, and sources. The formation of the subtemperate layer was due to the submerged flow formed when river water entered the reservoir, which provides a channel for DIC from the river to enter the lower layer of the reservoir. Human activities increased the solubility of carbonate rocks in the reservoir, and the source of DIC was one of the factors contributing to the concentration stratification of DIC in the reservoir.

Keywords: dissolved inorganic carbon; vertical transport; karst deep-water reservoirs; underflow; source



Citation: Zhou, Z.; Wang, C.; Li, Y.; Zhang, Y.; Kong, J. Vertical Divergence Characteristics of Dissolved Inorganic Carbon and Influencing Factors in a Karst Deep-Water Reservoir, Southwest China. *Atmosphere* **2023**, *14*, 1111. <https://doi.org/10.3390/atmos14071111>

Academic Editors: Xiaoyong Bai, Yongjun Jiang, Jian Ni, Xubo Gao, Yuemin Yue, Jiangbo Gao, Junbing Pu, Hu Ding, Qiong Xiao, Zhicai Zhang and Yoshizumi Kajii

Received: 4 May 2023

Revised: 22 June 2023

Accepted: 1 July 2023

Published: 4 July 2023



Copyright: © 2023 by the authors. Licensee MDPI, Basel, Switzerland. This article is an open access article distributed under the terms and conditions of the Creative Commons Attribution (CC BY) license (<https://creativecommons.org/licenses/by/4.0/>).

1. Introduction

Reservoirs play a significant role in regulating the climate [1,2] and changing engineering water scarcity [3]. The construction of reservoirs is a method of solving water scarcity in karst areas. As of 2020, there were 98,566 reservoirs in China of which 53% were large reservoirs and 58% were medium reservoirs in karst areas (<http://www.mwr.gov.cn/sj/>) (accessed on 30 June 2023). The construction of reservoirs has altered the continuity of rivers [4], affected the forms of biogenic elements [1,5] and the ecological environment [6], and changed the structure of water bodies, hydrological features, and community structure of aquatic organisms [7,8]. The mechanism of reservoir carbon cycling is different from that of river carbon cycling. Therefore, the study of reservoir carbon cycling has become a focus of carbon sink calculation and carbon balance studies [9,10].

Reservoirs play an important role in the exchange of matter and energy at the water–atmosphere interface [11], water–rock interface, and water–biological interface [12], as well as in carbon cycling and accumulation in watersheds [13], and they also play an important role in altering the carbon fluxes and pathways in river ecosystems [14]. In recent years, research on carbon cycling reservoirs has produced many results, for

example, the exploration of computational methods and models for reservoir carbon fluxes [15,16], the assessment of the carbon sink effects of river–reservoir systems [17,18], the study of the effects of thermal stratification, biological pumps, and chemical stratification on carbon cycling [14,19,20]. Reservoirs carbon transport models have confirmed that complex biogeochemical changes occur within reservoirs [14,20], including the conversion of inorganic carbon to organic carbon by photosynthesis of aquatic organisms [21], the degradation and mineralization of organic matter to produce inorganic carbon [22], bacteria producing CH₄ under anaerobic or sulphuric conditions [23–25], and the degassing of dissolved inorganic carbon (DIC) to produce CO₂ [26,27]. However, carbon exchange is limited by many factors [18], such as water residence time [28,29], water level [6], thermal stratification [30], chemical stratification [31], and reservoir age [32]. The above findings supported the construction of a reservoir carbon cycle model. However, the applicability of this carbon cycle model in karst areas is limited because of the vulnerability of carbon transport in karst areas to human activities and other factors [33].

DIC in reservoirs is from rock weathering, soil carbon loss [1,5], aquatic respiration [12], and water–air exchange [11]. The DIC concentration in a karst reservoir is significantly higher than in non-karst areas [17]. Aquatic plants can autotrophically convert DIC into organic carbon [21], some of which is permanently stored in the substrate and some of which is released into the atmosphere as CO₂ or CH₄ [22,34]. Because of the influence of the environment, DIC degassed to produce CO₂ and the carbonate precipitation DIC concentration is also important for the calculation of CO₂ fluxes at the water–gas interface. This suggests that the DIC is important for the carbon transport among the hydrosphere and the biosphere, atmosphere, and lithosphere. It is useful to better understand the carbon cycle and carbon balance in karst basins if studying the migration and transformation of the DIC.

Many researchers have started to study the migration and transformation of the DIC in karst reservoirs [20,35]. They have confirmed that thermal stratification is one of the main factors controlling changes in the DIC [36,37]. Current studies on DIC in karst reservoirs have mostly focused on the characteristics of the surface distribution and influencing factors. However, most reservoirs in karst areas are built according to the terrain and dammed in deep river valleys, so the water depth is mostly more than 30 m. These reservoirs are prone to thermal and chemical stratification in summer. The internal environment of these reservoirs is also more complex, with the water pressure, wind, and hydrodynamics all potentially leading to the exchange of the upper and lower water bodies, even during periods of thermal stratification. Therefore, a study of the characteristics of the vertical distribution and influencing factors of DIC in karst deep-water reservoirs is necessary for an in-depth study of the reservoir carbon cycle and carbon balance. In this study, 63 vertical profile samples were collected from the thermally stratified period to the mixed period in a deep-water reservoir in southwest China [38,39]. The spatial and temporal variation of the DIC concentration, partial pressure of CO₂ (pCO₂), and calcite saturation index (SI_c) were analyzed. The purpose was to investigate the divergence characteristics of the DIC in karst deep-water reservoirs in the vertical direction, influencing factors, and path of the DIC in river water into the reservoir.

2. Materials and Methods

2.1. Study Area

The study area is located at the Pingzhai Reservoir, a humid subtropical monsoon climate zone (105°17'57" E–105°25'50" E, 26°28'27" N–26°34'28" N), which is in Guizhou Province, southwest China (Figure 1a). The rainy season in the area is from May to October. The reservoir has a catchment area of 3249 km² of which 74.30% is a karst area. The main water source is the Sancha River, followed by the Shuigong, Zhangwei, Baishui, and Hujia rivers. The reservoir capacity is 1.09 × 10⁹ m³, and there is an underground reservoir with a capacity of 311 million m³, accounting for 29% of the total capacity of Pingzhai Reservoir [40]. In the catchment area, the main human activities are agriculture, residential

life, and industrial activities, and the mineral resources are coal and pyrite. The main land use types in the region are cropland, woodland, grassland, building land, water, and unused land (Figure 1c). The reservoir is a cyclic thermally stratified reservoir. It is in the mixed homogeneous phase from January to April, in the thermally stratified phase from May to October, in the thermally stratified stable phase from July to September, and in the mixing phase from November to December [40].

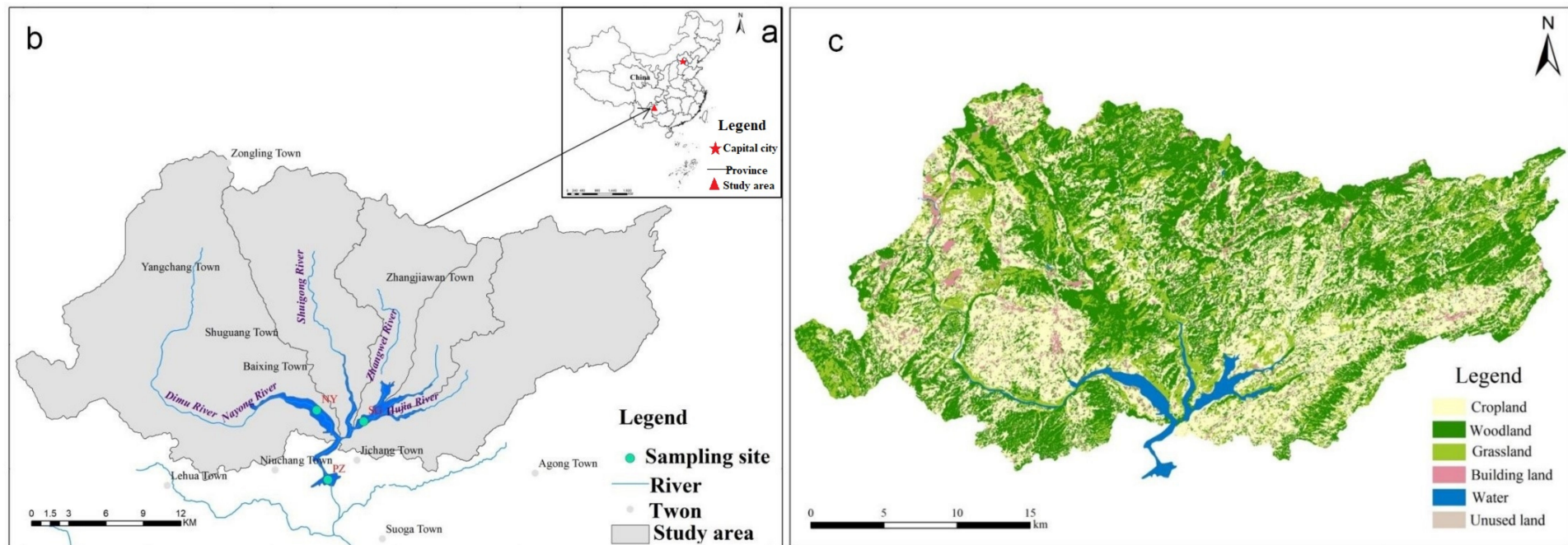


Figure 1. Map of the Pingzhai Reservoir showing the position of sampling points:(a) geographical location of the study area; (b) location of the sampling site; (c) land use in the study area.

2.2. Sample Collection and Analysis

According to the hydraulic connection and tributary distribution, NY, SG, and PZ were selected as the sampling sites (Figure 1b). The water temperature (T_{water}) and dissolved oxygen (DO) concentrations were measured every two or three months, from July 2019 to July 2021. Other indicators were measured every two months, from September 2019 to January 2020. During the sampling period, the minimum depth of the reservoir was 65 m, the maximum depth was 101 m, and the average depth was 87 m. Therefore, samples were collected at depths of 0.1, 10, 20, 30, 40, 50, and 60 m.

The study measured the T_{water} (± 0.01 °C), pH (± 0.01), electrical conductivity (EC; ± 1 mS cm^{-1}), DO concentration (± 0.01 mg·L $^{-1}$), chlorophyll a (chl-a) concentration, DIC isotopes ($\delta^{13}\text{C}_{\text{DIC}}$; measured values in thousandths (‰), analytical error < 0.2‰), the concentration of anions and cations (Ca^{2+} , Mg^{2+} , Na^+ , K^+ , HCO_3^- , CO_3^{2-} , SO_4^{2-} , NO_3^- , and Cl^-). T_{water} , DO, EC, and pH were measured using a Multi 3430 portable water quality analyzer (WTW Co. Ltd., Germany). The HCO_3^- and CO_3^{2-} concentrations were determined using acid–base kits (Aquamerck, Germany) (± 0.01 mg·L $^{-1}$). The samples for the anion and cation analysis were filtered through 0.45 μm cellulose acetate membrane and stored in HDPE bottles. Nitric acid was added to the samples for the cation analysis to bring the pH ≤ 2.0 . The samples of $\delta^{13}\text{C}_{\text{DIC}}$ were spiked with 3–5 drops of HgCl_2 solutions and stored in a polyethylene bottle without air bubbles. The cations were analyzed with ICP-EMS (relative error < 2%). The anions were analyzed using an ion spectrometer (IS90). The $\delta^{13}\text{C}_{\text{DIC}}$ was measured with a gas isotope mass spectrometer (MAT-252). A separate water sample of 500 mL was collected and stored in a brown glass bottle with the addition of magnesium carbonate suspension and kept at 4 °C in the dark; then, the chl-a concentration was measured with a spectrophotometer.

2.3. Data Processing

The α indicator method was used to determine the type of reservoir water temperature stratification [41].

$$\alpha = \frac{\text{Total inlet flow}}{\text{Total reservoir capacity}}$$

If $\alpha < 10$, the reservoir is a stable stratification type; if $10 \leq \alpha \leq 20$, it is a transitional type; if $\alpha > 20$, it is a mixed type.

In water, $p\text{CO}_2$ is the factor controlling the CO_2 exchange at the water–gas interface [42]. In this study, $p\text{CO}_2$ was calculated with Henry's law:

$$p\text{CO}_2 = [\text{H}_2\text{CO}_3^*]K_{\text{CO}_2} = \alpha (\text{H}^+) \cdot \alpha (\text{HCO}_3^-) K_{\text{CO}_2} \times K_1$$

In Equation, α is the ionic activity, K_{CO_2} is Henry's constant, and K_1 is the first dissociation constant.

SIC is the indicator to determine the state of reaction between water and carbonate rock. $SIC = 0$, $SIC < 0$, and $SIC > 0$ denote dissolution equilibrium, precipitation, and erosion of carbonate rocks, respectively [43]. In this study, SIC was calculated by Phreeqc3.1.7:

$$SIC = \text{Log}(IAP/K_{\text{cal}})$$

In this equation, IAP is ionic activity, and K_{cal} is the equilibrium constant of calcite dissolution.

3. Results

3.1. Characteristics of T_{water} , DO Changes, and Reservoir Thermal Stratification Patterns

In the Pingzhai Reservoir, T_{water} decreased with the water depth. The highest T_{water} was 27.60 °C at the surface layer, and the lowest T_{water} was 10.75 °C at the 60 m depth. The T_{water} varied significantly from the surface layer to 20 m depth. However, it changed slightly at depths of 50 m and below. The T_{water} in the upper layer showed an annual cycle

of variation. The T_{water} was lowest in January, then warmed up to a maximum in July, and then gradually decreased (Figure 2a–c). The cyclical variation of the T_{water} in Pingzhai Reservoir is mainly influenced by solar radiation.

The variability of DO concentration was more complex than that of T_{water} and did not follow an annual cycle. The DO concentrations were higher in the upper layer than in the lower layer and increased in the surface layer between January and July but decreased significantly at depths of 10 m and 20 m. The lowest DO concentrations occurred in May and were less than 2.0 mg/L (Figure 2d–f). This is consistent with the climate trends in the Pingzhai Reservoir basin and the distribution characteristics of algae in the reservoir.

The values of α were calculated with the data collected at the Yangchang Hydrological Station from 2014 to 2019. The total inflow of Pingzhai Reservoir was 1348 million m^3/a , the capacity was $1.09 \times 10^9 \text{ m}^3$. The result shows that α was 1.19 and was less than 10. Therefore, the Pingzhai Reservoir was stably stratified. Combined with the variation of the T_{water} , thermal stratification in the Pingzhai Reservoir occurs from April to September, while the upper and lower T_{water} is consistent in January. Using a temperature difference of $0.2 \text{ }^\circ\text{C}/\text{m}$ to assess the thermal stratification [43], the thermocline occurs below the surface to a depth of 10 m. However, from April to November there is a temperature difference of more than $0.2 \text{ }^\circ\text{C}/\text{m}$ at a depth of 20 to 50 m. It makes the Pingzhai Reservoir a double thermocline reservoir.

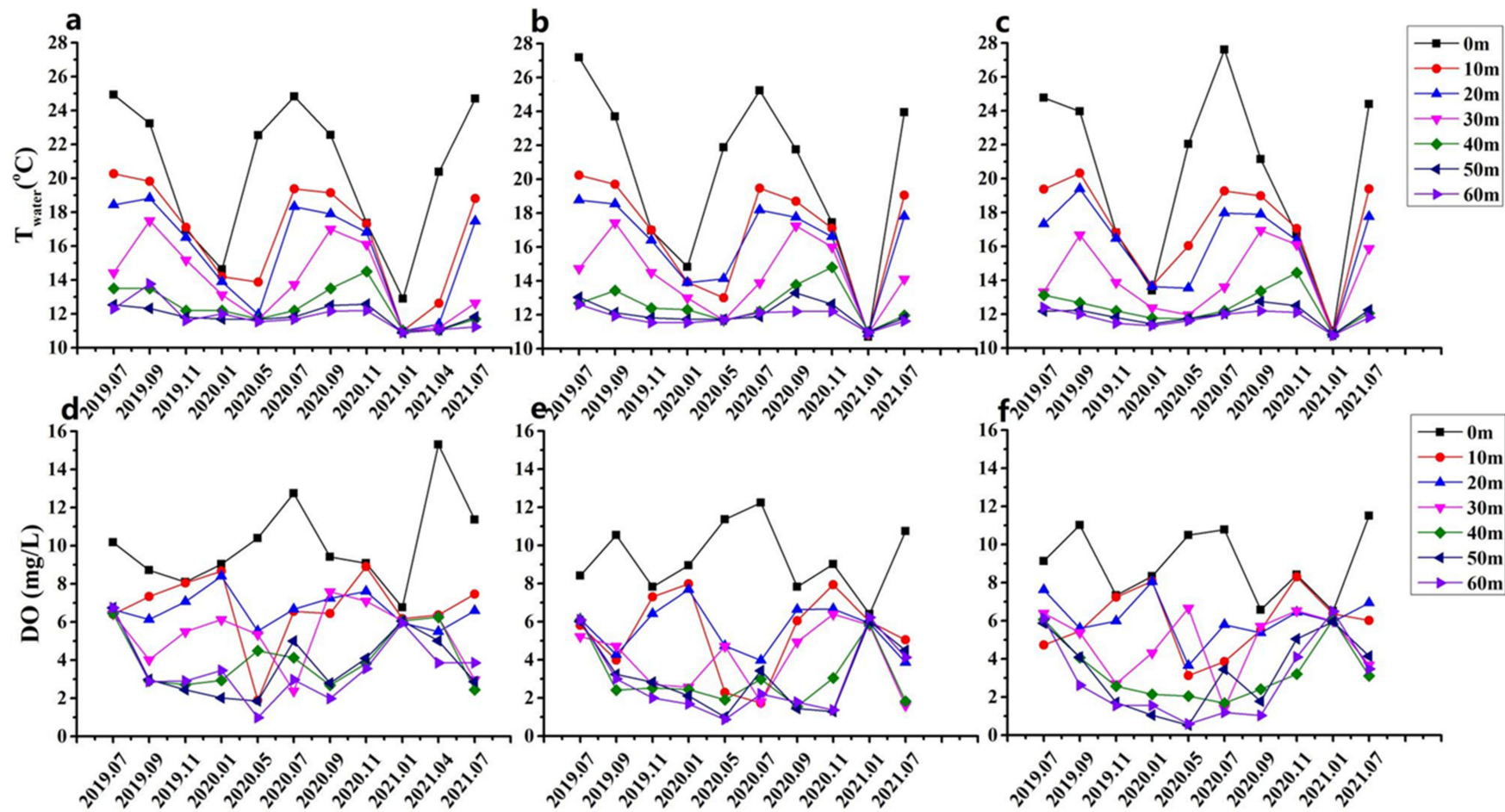


Figure 2. Temporal and spatial variation of water temperature and DO concentration in Pingzhai Reservoir: (a–c) T_{water} at the NY, PZ, and SG sites, respectively; (d–f) DO concentration at the NY, PZ, and SG sites, respectively.

3.2. Distribution Characteristics of DIC and Vertical Variation of $\delta^{13}C_{DIC}$

The DIC is composed of H_2CO_3 , HCO_3^- , and CO_3^{2-} . In the Pingzhai Reservoir, the pH was 7.50–9.01, where approximately 98% of the DIC was HCO_3^- , and the HCO_3^- concentration was often used to characterize the DIC concentration in the water column [44]. In the Pingzhai Reservoir, the DIC concentration was 76.25–204.35 mg. The mean concentration was 168.43 mg L^{-1} , which is consistent with the DIC concentration in other karst areas [42,45]. Vertically, the DIC concentration increased with the water depth from the surface layer to the 40 m depth. From the 40 m to 60 m depth, the DIC concentration varied slightly. The analysis of the coefficient of variation showed that the DIC concentration varied greatly in the upper layer and less in the lower layer, especially in the 50 m and 60 m depths where the coefficient of variation was the lowest. The analysis of the coefficients of the variation for the different phases at the NY, PZ, and SG sites showed that the variation of the DIC concentration was thermal stratification phase > mixing phase > mixed phase. In the thermal stratification phase, the spatial variation of the DIC concentration was $SG > PZ > NY$. In the mixing and mixed phases, the spatial variation of the DIC concentration was $SG > NY > PZ$ in (Figure 3a).

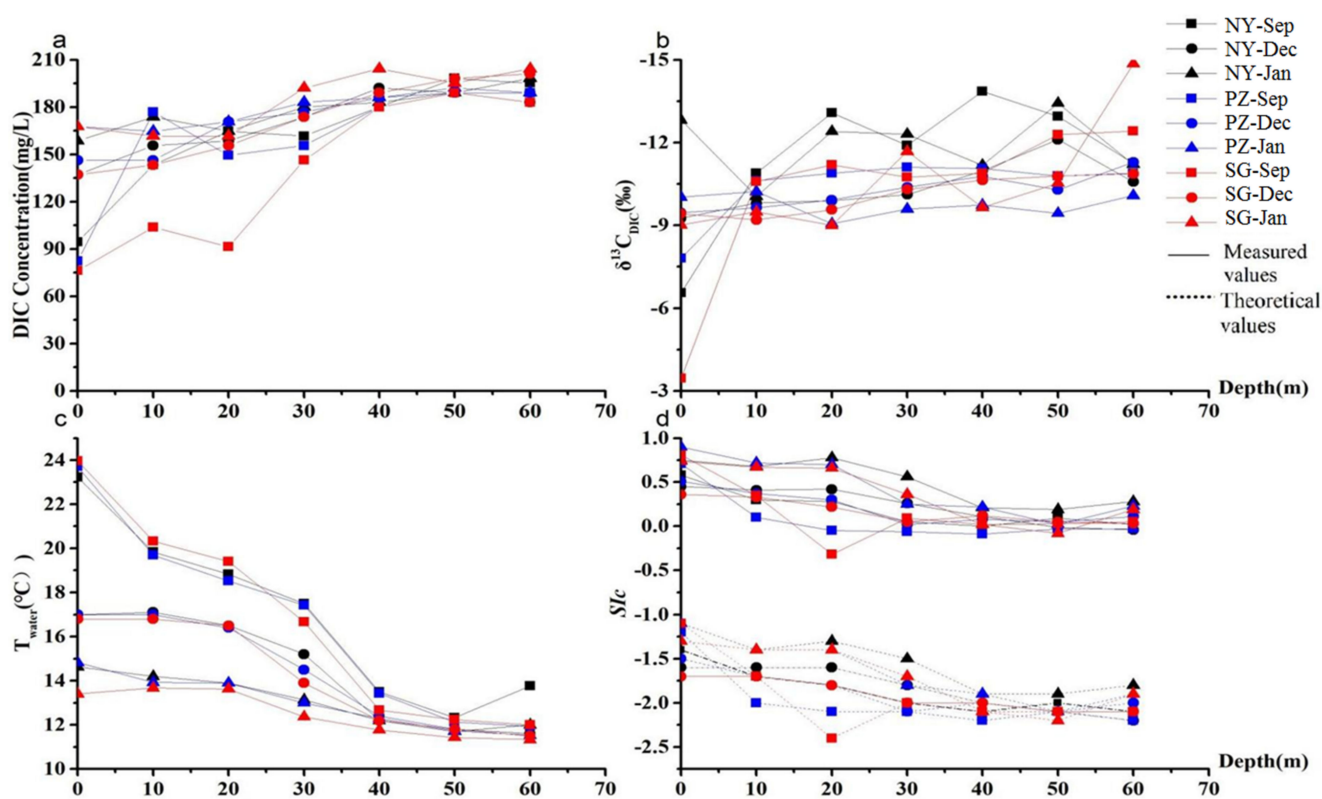


Figure 3. DIC concentration, $\delta^{13}C_{DIC}$ value, T_{water} , and SiC vary in the vertical direction: (a) change in the DIC concentration in the vertical direction; (b) change in the $\delta^{13}C_{DIC}$ value in the vertical direction; (c) change of T_{water} in the vertical direction; (d) change in the SiC in the vertical direction.

In the Pingzhai Reservoir, the $\delta^{13}C_{DIC}$ values ranged from -3.454‰ to -14.857‰ . The mean $\delta^{13}C_{DIC}$ values in the thermal stratification phase, mixing phase, and mixed phases were -10.726‰ , -10.254‰ , and -10.751‰ , respectively. Only the surface $\delta^{13}C_{DIC}$ value of the thermal stratification phase was greater than -8‰ , while the rest were less than -9‰ . In the 10 m–60 m depth range, the $\delta^{13}C_{DIC}$ values ranged from -9‰ to -12‰ (Figure 3b). A statistical analysis of the $\delta^{13}C_{DIC}$ values also showed that there was a significant difference between the surface and lower layers in the thermal stratification phase, while there was no significant difference between the mixing and mixed phases. The

changing trends between the $\delta^{13}\text{C}_{\text{DIC}}$ values and T_{water} indicated that the lower the T_{water} , the more the $\delta^{13}\text{C}_{\text{DIC}}$ values were overweighted (Figure 3b,c).

The Ca^{2+} , Mg^{2+} , and DIC are indicators of carbonate rock weathering. The K^{+} and Na^{+} are indicators of silicate rock weathering. The Cl^{-} , SO_4^{2-} , and NO_3^{-} are indicators of human activities. The Chl-a is an indicator of aquatic plants. The pH and DO are indicators of the water environment. The correlation analysis showed that carbonate weathering and silicate weathering occurred simultaneously. The salinity effect caused increased solubility of ions in the reservoir and an increased ion concentration. Human activities also affected the pH and hence the weathering of the carbonate rocks. As algae are the main actors in carbon transport from the biosphere to the atmosphere and hydrosphere, they are highly significantly correlated with DIC, while pH and DO affect algal abundance, on the one hand, and carbon exchange at the water–air interface on the other (Table 1). This shows that the DIC concentration in the reservoir was influenced by rock weathering, human activities, aquatics, and the nature of the water column.

Table 1. Correlation analysis of each index in Pingzhai Reservoir.

	Ca^{2+}	K^{+}	Mg^{2+}	Na^{+}	Cl^{-}	NO_3^{-}	SO_4^{2-}	DIC	pH	$\delta^{13}\text{C}_{\text{DIC}}$	DO	Chl-a
Ca^{2+}	1											
K^{+}	0.573 **	1										
Mg^{2+}	0.470 **	0.932 **	1									
Na^{+}	0.288 *	0.810 **	0.845 **	1								
Cl^{-}	0.209	0.488 **	0.523 **	0.684 **	1							
NO_3^{-}	0.576 **	0.271	0.165	−0.133	0.098	1						
SO_4^{2-}	0.408 **	0.538 **	0.607 **	0.586 **	0.894 **	0.362 **	1					
DIC	0.363 **	0.120	0.175	0.038	0.171	0.336 *	0.365 **	1				
pH	−0.227	0.036	0.149	0.244	0.002	−0.363 **	−0.065	−0.425 **	1			
$\delta^{13}\text{C}_{\text{DIC}}$	−0.684 **	−0.436 **	−0.325 *	−0.046	−0.074	−0.684 **	−0.267	−0.272	0.463 **	1		
DO	−0.091	0.054	0.095	0.077	−0.172	−0.096	−0.166	−0.310 *	0.863 **	0.214	1	
Chl-a	0.151	−0.063	−0.058	−0.185	0.003	0.211	0.092	0.489 **	−0.152	−0.231	0.045	1

* $p < 0.05$, ** $p < 0.01$.

However, the stratified correlation analysis showed that the DIC concentrations varied at different depths. The surface DIC concentration was influenced by carbonate weathering and human activities but also by the temperature and atmospheric CO_2 concentrations. The DIC concentration at the 30 m depth was influenced by carbonate and silicate weathering and human activities. The DIC concentrations at the 10 m, 50 m, and 60 m DIC concentrations were not significantly affected. The DIC concentration at the 20 m and 40 m depths were influenced by Na^{+} and water temperature, respectively (Table 2).

Table 2. Correlation analysis between DIC and water chemistry and environmental factors at different depths.

	Surface Layer	10 m Depth	20 m Depth	30 m Depth	40 m Depth	50 m Depth	60 m Depth
Ca^{2+}	0.885 **	0.273	0.4	0.706 *	0.188	0.371	0.491
Mg^{2+}	0.627	0.078	0.633	0.832 **	−0.58	−0.381	0.253
K^{+}	0.545	−0.035	0.293	0.691 *	−0.654	−0.455	0.229
Na^{+}	0.411	0.099	0.680 *	0.836 **	−0.593	−0.428	0.256
Cl^{-}	0.138	−0.079	0.366	0.888 **	−0.26	−0.333	−0.325
NO_3^{-}	0.915 **	−0.172	−0.279	−0.14	0.317	−0.286	−0.215
SO_4^{2-}	0.299	−0.035	0.534	0.837 **	0.089	−0.373	−0.191
T_{water}	−0.989 **	−0.539	−0.597	−0.903 **	−0.760 *	0.01	−0.005
DO	−0.671 *	0.211	0.445	−0.291	−0.551	−0.432	−0.344
pH	−0.780 *	0.063	0.506	0.417	0.555	−0.187	0.073
chl-a	−0.662	0.105	0.17	−0.581	−0.447	0.289	−0.518
Humidity	−0.328	-	-	-	-	-	-
Wind speed	0.048	-	-	-	-	-	-
Air temperature	−0.811 **	-	-	-	-	-	-
Barometric pressure	0.499	-	-	-	-	-	-
Atmospheric CO_2 concentration	0.879 **	-	-	-	-	-	-

* $p < 0.05$, ** $p < 0.01$.

3.3. Characteristics of SIc and pCO_2 Variation in the Pingzhai Reservoir

SIc is an indicator of the weathering tendency of carbonate rocks. When $SIc > 0$, carbonate rocks are precipitating; when $SIc < 0$, carbonate rocks are dissolving; when $SIc = 0$, the dissolution reaction of carbonate rocks reaches equilibrium. In the Pingzhai Reservoir, SIc ranged from -0.09 to 0.90 . SIc were high in the surface layer and decreased with the water depth. The SIc were positive for all phases, sites, and depths, except for depths below 20 m at the PZ site during the thermal stratification phase, depths below 50 m at the NY site during the mixing phase, and depths below 50 m at the SG site during the mixed phase. Most of the time, the carbonate concentration was supersaturated (Figure 3d). The correlation analysis showed that a SIc above 30 m depth was significantly positively correlated with pH, Na^+ , DO, and Mg^{2+} ($p < 0.01$) and significantly negatively correlated with T_{water} ($p < 0.01$). Below 30 m depth, SIc was significantly positively correlated with pH, Ca^{2+} , Na^+ , Mg^{2+} , K^+ , SO_4^{2-} , and EC ($p < 0.01$ or $p < 0.05$) and negatively correlated with chl-a ($p < 0.05$) (Table 3).

Table 3. Correlation analysis between SIc and water chemistry and environmental factors at different depths.

	Surface Layer	10 m Depth	20 m Depth	30 m Depth	40 m Depth	50 m Depth	60 m Depth
Ca^{2+}	0.373	0.468	0.519	0.705 *	0.464	0.268	0.921 **
Mg^{2+}	0.51	0.043	0.826 **	0.875 **	0.628	0.832 **	0.878 **
K^+	0.645	0.009	0.532	0.778*	0.541	0.799 **	0.830 **
Na^+	0.733 *	0.204	0.895 **	0.902 **	0.599	0.764 *	0.824 **
Cl^-	0.594	-0.406	0.245	0.869 **	-0.085	0.525	-0.603
NO_3^-	0.258	-0.505	-0.467	0.082	-0.157	0.613	-0.224
SO_4^{2-}	0.578	-0.377	0.307	0.832 **	0.409	0.307	-0.374
T_{water}	0.014	-0.889 **	-0.911 **	-0.694 *	-0.618	0.192	-0.253
DO	0.681 *	0.792 *	0.889 **	0.461	-0.06	0.116	-0.181
EC	0.105	0.006	0.489	0.802 **	0.268	-0.161	0.172
pH	0.585	0.897 **	0.924 **	0.933 **	0.804 **	0.175	0.877 **
chl-a	-0.204	-0.585	-0.136	-0.682 *	-0.695 *	0.1	-0.712 *
Humidity	-0.533	-	-	-	-	-	-
Wind speed	-0.263	-	-	-	-	-	-
Air temperature	0.347	-	-	-	-	-	-
Barometric pressure	-0.596	-	-	-	-	-	-
Atmospheric CO_2 concentration	-0.271	-	-	-	-	-	-

* $p < 0.05$, ** $p < 0.01$.

pCO_2 is an indicator that determines the direction of carbon transport at the water–air interface and calculates exchange fluxes. In the Pingzhai Reservoir, pCO_2 increased with the water depth. Its changing tendency was opposite to that of T_{water} and the same as that of DIC. The response of pCO_2 to the water depth lagged behind that of DIC. The surface pCO_2 ranged from 4.74 Pa to 61.05 Pa (Figure 4), while the atmospheric pCO_2 ranged from 25.2 Pa to 30.6 Pa. The atmospheric pCO_2 was larger than the surface pCO_2 in the thermal stratification phase but smaller than the surface pCO_2 in the mixing and mixed phases. The correlation analysis showed that the surface pCO_2 was significantly negatively correlated with T_{water} , pH, DO, and air temperature ($p < 0.01$) and positively correlated with atmospheric pCO_2 ($p < 0.01$) and barometric pressure ($p < 0.05$). Below the surface, pCO_2 was not influenced by atmospheric parameters. At different depths, different factors were significantly correlated with pCO_2 (Table 4).

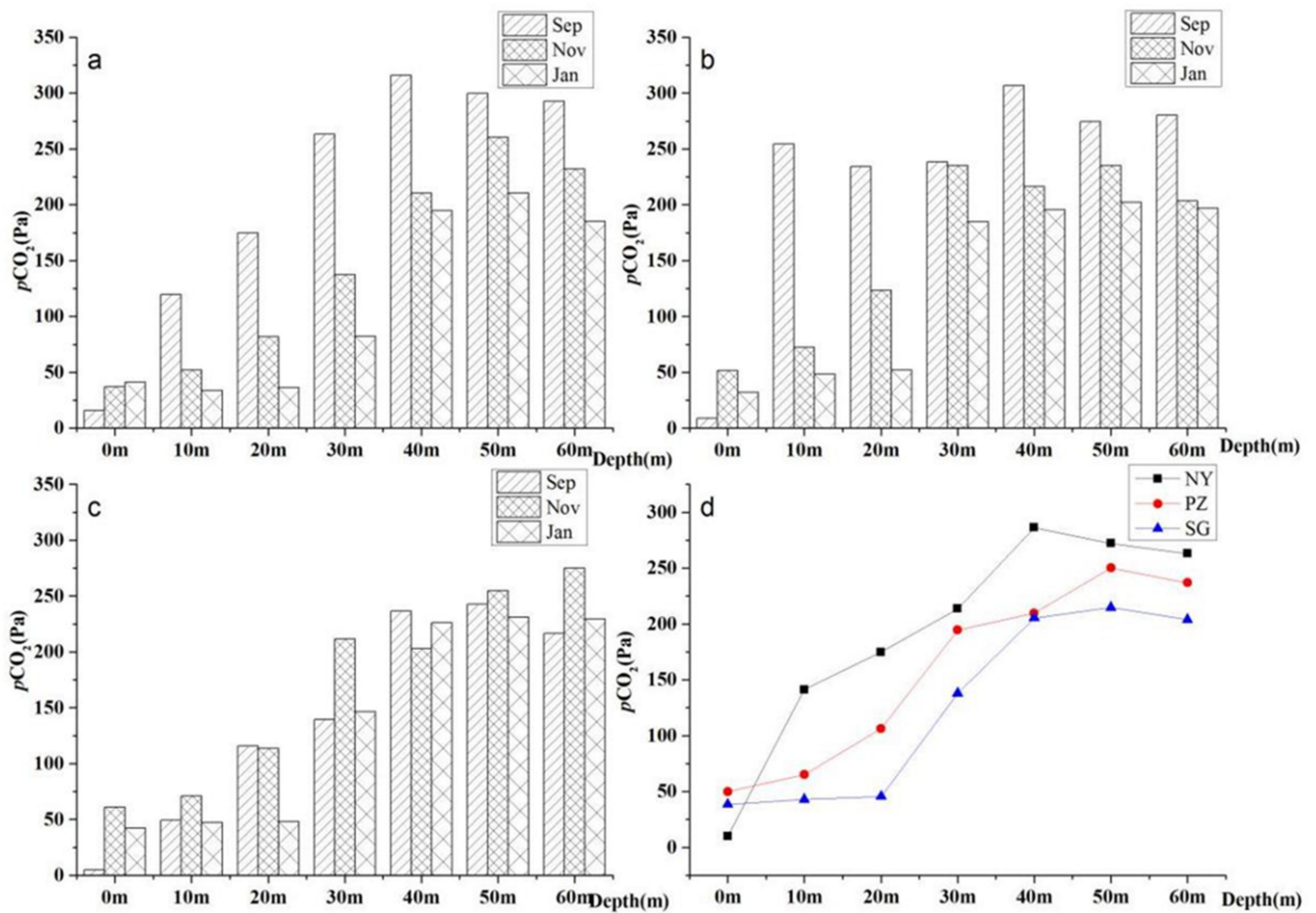


Figure 4. Variation in the vertical profile of the partial pressure of carbon dioxide (pCO₂) in the Pingzhai Reservoir, China: (a–c) NY, PZ, and SG sites, respectively; (d) mean value of each points.

Table 4. Correlation analysis between pCO₂ and water chemistry and environmental factors at different depths.

	Surface Layer	10 m Depth	20 m Depth	30 m Depth	40 m Depth	50 m Depth	60 m Depth
Ca ²⁺	0.547	0.017	−0.198	−0.269	−0.146	−0.338	−0.505
Mg ²⁺	0.125	0.285	−0.508	−0.546	−0.368	0.047	−0.646
K ⁺	−0.002	0.239	−0.305	−0.393	−0.241	0.109	−0.587
Na ⁺	−0.119	0.147	−0.625	−0.622	−0.358	0.174	−0.541
Cl [−]	−0.353	0.3	0.037	−0.526	−0.083	0.153	0.525
NO ₃ [−]	0.566	0.337	0.618	0.165	−0.099	0.117	0.246
SO ₄ ^{2−}	−0.225	0.357	0.207	−0.443	−0.418	−0.424	0.433
Twater	−0.803 **	0.567	0.816 **	0.509	0.898 **	0.692 *	0.505
DO	−0.894 **	−0.791 *	−0.928 **	−0.659	0.056	0.391	0.035
EC	0.614	0.383	0.017	−0.412	−0.432	−0.472	0.042
pH	−0.962 **	−0.906 **	−0.909 **	−0.972 **	−0.987 **	−0.981 **	−0.962 **
chl-a	−0.556	0.394	0.44	0.704*	0.905 **	0.793 *	0.534
Humidity	−0.059	-	-	-	-	-	-
Wind speed	0.294	-	-	-	-	-	-
Air temperature	−0.851 **	-	-	-	-	-	-
Barometric pressure	0.796 *	-	-	-	-	-	-
Atmospheric CO ₂ concentration	0.867 **	-	-	-	-	-	-

* $p < 0.05$, ** $p < 0.01$.

There were also spatial and temporal differences in the pCO₂ (Figure 4). At the surface, pCO₂ was generally NY < SG < PZ. However, below the surface, it was SG < PZ < NY.

Apart from the surface layer, $p\text{CO}_2$ also showed some temporal patterns of variation. At the NY and PZ sites, $p\text{CO}_2$ generally showed a thermal stratification phase > mixing phase > mixed phase, while SG showed no clear temporal pattern. The maximum $p\text{CO}_2$ at the PZ and NY sites during the thermal stratification phase was at a depth of 40 m, while at the SG site, it was at a depth of 50 m. The maximum $p\text{CO}_2$ was at a depth of 50 m for the NY and PZ sites and 60 m for the SG site during the mixing and mixed phases.

3.4. DIC Sources in Pingzhai Reservoir

Ca^{2+} was the most dominant cation in Pingzhai Reservoir, accounting for 57.7% to 82.53% of the total cation concentration. SO_4^{2-} was the second most dominant anion, accounting for 20.05% to 41.04% of the total anion concentration. The ratios of $(\text{Ca}^{2+} + \text{Mg}^{2+})/(\text{HCO}_3^- + \text{SO}_4^{2-})$ and $(\text{Ca}^{2+} + \text{Mg}^{2+})/(\text{HCO}_3^-)$ were both approximately 1 (Figure 5), with significant correlation coefficients of 0.71 and 0.69, respectively. The results indicate that carbonate weathering controlled the water chemistry and DIC correlated with Ca^{2+} , Mg^{2+} , and SO_4^{2-} (Figure 6).

In the Wujiang River basin, the $\delta^{13}\text{C}_{\text{DIC}}$ from soil organic matter formation ranged from -16‰ to -19‰ [46], from carbonate rock weathering ranged from -2‰ to 2‰ [45], and from atmospheric CO_2 dissolved in water was about $0\sim 2.5\text{‰}$ [38]. In the Pingzhai Reservoir, the $\delta^{13}\text{C}_{\text{DIC}}$ ranged from -3.454‰ to -14.857‰ . Therefore, based on the water chemistry and isotopic analysis, the DIC was mainly derived from soil organic matter and carbonate rock weathering. Based on the ^{13}C mass balance principle [47], approximately 60.44% of the DIC was derived from soil organic matter, 14.78% from carbonate rock and 14.78% from atmosphere. However, the source of DIC varies spatially and seasonally. The NY site was 64.40% from soil organic matter and with the soil source being 5–6 percentage points higher than other points; DIC in the thermal stratification phase had approximately 33.93% from soil and 33.04% from carbonate rock and 33.03% from atmosphere.

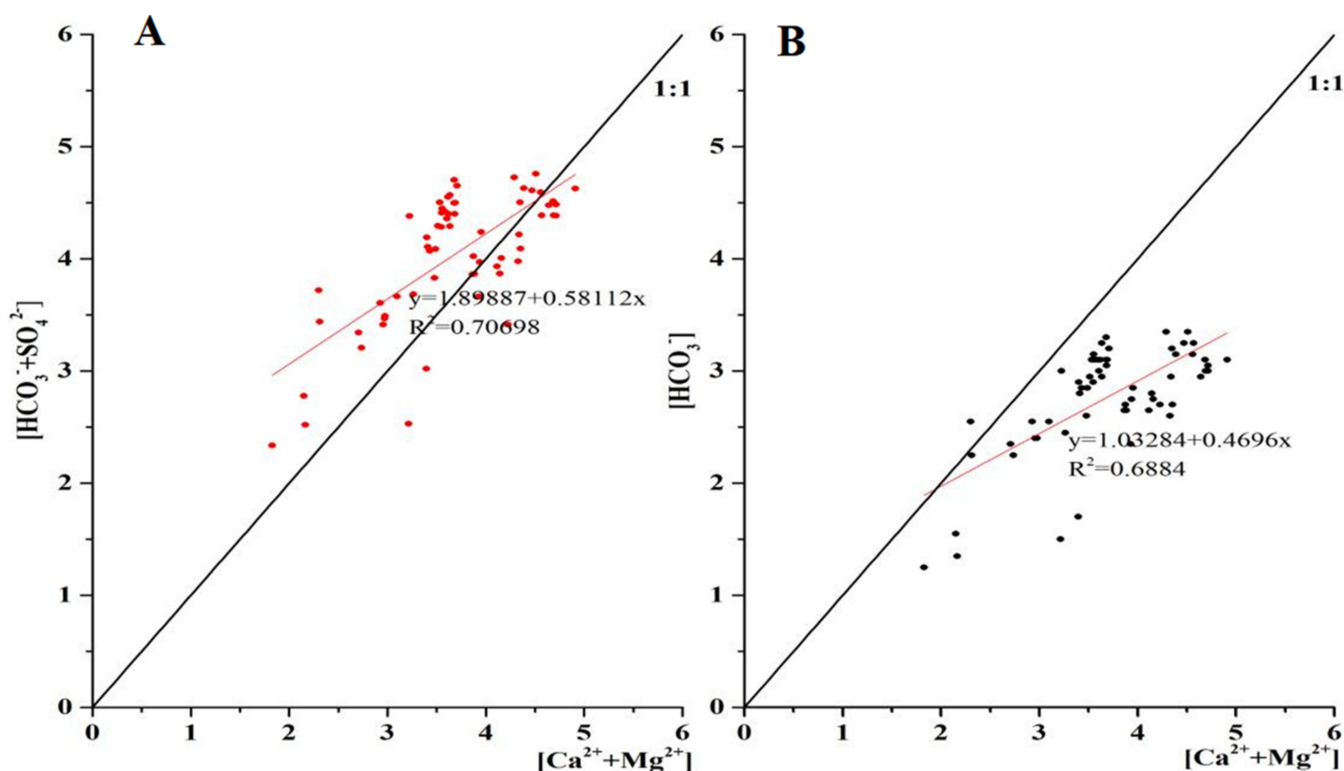


Figure 5. Equivalence ratios of ions in the Pingzhai Reservoir, China. ((A) is the ratio of $[\text{Ca}^{2+} + \text{Mg}^{2+}]$ to $[\text{HCO}_3^- + \text{SO}_4^{2-}]$, (B) is the ratio of $[\text{Ca}^{2+} + \text{Mg}^{2+}]$ to $[\text{HCO}_3^-]$).

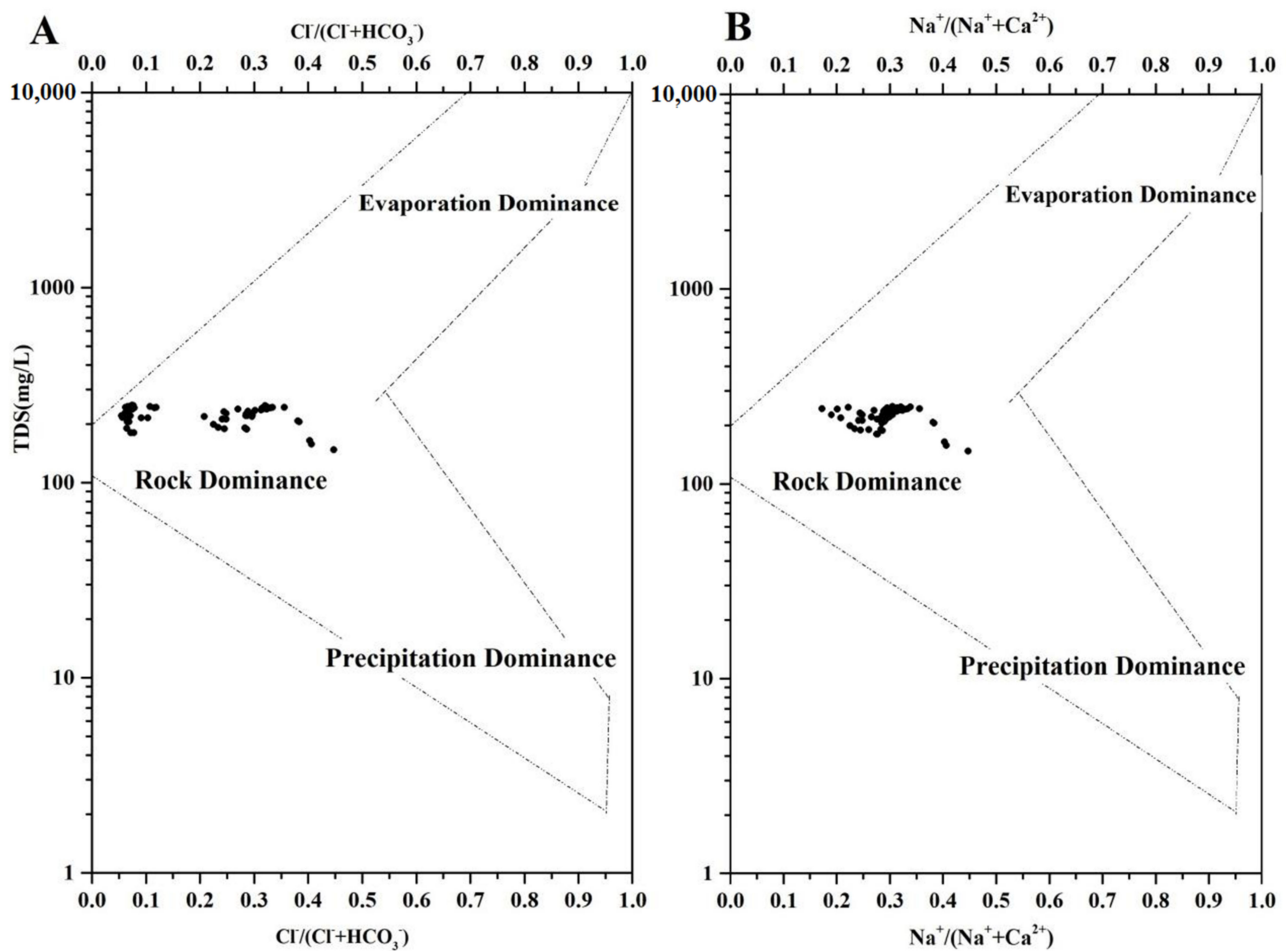


Figure 6. Gibbs chart showing the vertical distribution of anions (A) and cations (B) in the Pingzhai Reservoir, China.

4. Discussion

4.1. Mechanism of Subthermocline Formation and Its Influence on the Vertical Distribution of DIC

Studies have shown that thermal stratification is the dominant factor leading to the vertical differentiation of DIC in deep karst reservoir [42]. There are two thermal layers in the Pingzhai Reservoir, the surface to 10 m depth is the main thermal layer, which is about 10 m thick. Between the 30 m depth and 50 m depth, there is a secondary thermal layer the thickness of which varies between 10 and 20 m. The formation mechanism of the main thermocline is solar radiation, the same as that of the other reservoirs in the Wujiang watershed. But this influence decreases below 10 m. However, the formation mechanism of the secondary thermocline is not clear [48]. Previous studies have shown that the thermocline impedes material exchange, and phytoplankton from the surface layer of the reservoir cannot reach the lower layer [30]. However, in the Pingzhai Reservoir, chl-a was detected in the lower layer and affected pCO_2 and Sic below a 30 m depth (Tables 3 and 4). The DIC concentration, pCO_2 , and Sic at a 30 m depth was significantly correlated with Ca^{2+} , Mg^{2+} , pH, and chl-a (Tables 2–4). During the thermally stratified phase, the tributaries of the Pingzhai Reservoir had the largest volumes and flow rates. Because of the inertial flow, the river forms a mainstem below the surface with a higher flow velocity than the surface layer [49]. In addition, the main flow is from west to east, and it is easier for the river to form a subduction below the reservoir surface under the Coriolis forces [49,50]. $\delta^{13}C_{DIC}$ analysis shows that the $\delta^{13}C_{DIC}$ in the reservoir at 30 m to 50 m depth is closer to the $\delta^{13}C_{DIC}$ from the soil. The formation of the subtemperate layer at 50 m is due to the formation of the para-temperate layer at 50 m caused by the

downward flow of river water into the reservoir. This result further confirms that at the Pingzhai Reservoir, the river water forms a subduction into the reservoir below the surface layer due to a combination of inertial action and Coriolis forces as it enters the reservoir. The material in the river water also enters the lower reservoir layer with the submerged flow. Thus, although thermal stratification controls the vertical partitioning characteristics of DIC in Pingzhai Reservoir, the variability of river DIC in the vertical direction is more complex due to changes in the mixed diffusion pattern of river water entering the reservoir. The sampling interval of 10 m in this study was not sufficiently accurate in determining the thickness of the subthermal layer and the hydraulic characteristics of the submerged flow, and further research is needed.

4.2. Source Influences the Vertical Difference in DIC Concentration

In this study, the DIC concentration was significantly correlated with the DIC source fraction (Table 5), indicating that the DIC source influenced the variation of DIC concentration. During the thermal stratification phase, the percentage of DIC from carbonate rocks and atmospheric was high, the $\delta^{13}\text{C}_{\text{DIC}}$ value in the surface layer was about -8% , while the DIC was readily available to aquatic plants for photosynthesis [51]. The DIC from soil was negative and more likely to enter the lower layer of the reservoir with the submerged flow, so the DIC concentration in the surface layer was significantly lower than that in the subsurface layer. During the mixing and mixed phases, DIC from the soil was dominant. It did not have the advantage of being used by photosynthesis [52]. Therefore the DIC concentration from the river did not change in the reservoir except for mixing, and no stratification of DIC concentration occurred. Some studies show that the surface T_{water} was higher than the lower layer in winter, the density of surface water was greater than the lower layer and the sinking of the upper layer of water under the action of gravity was the main mechanism of reservoir overtopping and consistent DIC concentration in reservoir [50]. However, in the Pingzhai Reservoir, the surface T_{water} exceeds $10\text{ }^{\circ}\text{C}$ in autumn and winter, and the surface T_{water} is still higher than the lower layer, so the density of the upper layer is lower than that of the lower layer. Therefore, in the Pingzhai Reservoir, the reflux gradient flow is the main mechanism of the water mixing in the upper and lower layers of the reservoir [53,54], and the gradual decrease in the pCO_2 in the reservoir from the bottom to the surface layers (Figure 4) confirms the existence of this mechanism. Thus, the different sources of DIC influence whether DIC concentration stratification occurs in the reservoir.

Table 5. Correlation analysis of the DIC, SO_4^{2-} , and NO_3^- concentrations with the source proportions.

	DIC (mg/L)	SO_4^{2-} (mg/L)	NO_3^- (mg/L)
Sources of carbonate rock	-0.548^{**}	-0.335	-0.492^{**}
Sources of soil organic matter	0.548^{**}	0.335	0.492^{**}
Sources of air	-0.548	-0.335	-0.492

** $p < 0.01$.

The surface layer is denser than the lower layer, and the sinking of the upper layer is the main mechanism for the reservoir overturning [50]. However, in the Pingzhai Reservoir, the surface T_{water} is more than $10\text{ }^{\circ}\text{C}$ in autumn and winter, and the T_{water} in the surface layer is still higher than that in the lower layer, so the density of the upper layer is lower than that of the lower layer. The overturning of the reservoir cannot be achieved. Therefore, the difference in the DIC sources affects the DIC concentration in the vertical direction.

4.3. Impact of Human Activities on DIC Concentration in the Reservoir

There are many human activities in the upstream watershed of the Pingzhai Reservoir, including industrial activities related to pyrite and coal, agricultural activities related to farming, and residential production and living. In the reservoir, $\text{SO}_4^{2-}/\text{Na}^+$ ranged from 2.11 to 7.00 and $\text{NO}_3^-/\text{Na}^+$ ranged from 0.27 to 1.74 (Table 6), both between agricultural and industrial activity

input end elements [55]. This indicated that human activities affected the water chemistry. SO_4^{2-} was the second most abundant anion in the Pingzhai Reservoir, accounting for 20.05% to 41.04% of the total anions. The ratio of $(\text{Ca}^{2+} + \text{Mg}^{2+})/(\text{HCO}_3^- + \text{SO}_4^{2-})$ was about 1 (Figure 5A). The relationships between SO_4^{2-} , NO_3^- , DIC, Ca^{2+} , and Mg^{2+} suggested that SO_4^{2-} and NO_3^- were involved in the weathering of the carbonate rocks (Table 1).

Table 6. Statistical table of major ion concentration ratios.

	Cl^-/Na^+	$\text{SO}_4^{2-}/\text{Na}^+$	$\text{NO}_3^-/\text{Na}^+$
Min. value	0.164	2.116	0.276
Max. value	0.782	7.001	1.743
Mean value	0.491	4.320	0.870
Standard deviation	0.098	0.858	0.276
Coefficient of variation	0.200	0.199	0.317
Critical Value of significant (<i>t</i> -test)	0.516	4.536	0.940
Critical value of highly significant (<i>t</i> -test)	0.525	4.607	0.963

Studies on the anthropocentric involvement of sulfuric and nitric acids in the weathering of carbonate rocks suggest two mechanisms of involvement, one in the form of acids [56,57], and the other being in a salt effect in the presence of $\text{SO}_4^{2-}/\text{NO}_3^-$ which increases the solubility of the carbonate rock, rather than a shift in the weathering equilibrium of the carbonate rock [58]. The pH of the Pingzhai Reservoir is 7.50 to 9.01, so sulfur and nitrogen were imported into the reservoir as ions rather than acids. In the reservoir area, the influx of SO_4^{2-} and NO_3^- increased the dissociation of carbonate rocks, which supersaturated the Sic of Pingzhai Reservoir (Figure 3d).

The supersaturated DIC concentration was susceptible to change, especially in the surface layer in the reservoir by climatic and hydrological changes, such as aquatic absorbed DIC to generate O_2 , the DIC degassed to produce CO_2 discharge into the air. This further explains that the DIC concentrations in the lower layer are higher than that in the subsurface layer. The ratios of $\text{SO}_4^{2-}/\text{Na}^+$ and $\text{NO}_3^-/\text{Na}^+$ in the surface layer were higher than those in the lower layer, indicating that human activities had greater impact on the water chemistry in the surface layer than in the lower layer [59], affecting the vertical partitioning of DIC in the reservoir.

5. Conclusions

Pingzhai Reservoir is a doublethermocline reservoir. The underflow is the factor leading to the formation of the subthermocline. The concentration of the DIC was lower in the surface layer and higher in the lower layer, while pCO_2 generally increased with depth and Sic gradually decreased with depth. The subthermocline, human activities, and the source of DIC all influence the vertical divergence of DIC concentrations. In particular, the presence of the subtemperate layer allows the DIC in rivers to enter the lower reservoir layer directly through the subtemperate layer channel.

Author Contributions: Conceptualization, Z.Z. and C.W.; methodology, Z.Z.; formal analysis, Z.Z. and C.W.; investigation, Y.L. and J.K.; resources, Z.Z.; data curation, Y.Z.; writing—original draft preparation, C.W.; writing—review and editing, Z.Z.; visualization, Y.Z.; project administration, C.W.; funding acquisition, Z.Z. All authors have read and agreed to the published version of the manuscript.

Funding: This work was supported by the National Natural Science Foundation of China (No. 42161048); Guizhou Science and Technology Program (No. (20201Y154)).

Institutional Review Board Statement: Not applicable.

Informed Consent Statement: Not applicable.

Data Availability Statement: The data presented in this study are available on request from the corresponding author.

Acknowledgments: The authors would like to thank the editors and the anonymous reviewers for their valuable comments and suggestions on this paper.

Conflicts of Interest: The authors declare no conflict of interest.

References

1. Hughes, H.J.; Bouillon, S.; Andre, L.; Cardinal, D. The effects of weathering variability and anthropogenic pressures upon silicon cycling in an intertropical watershed (Tana River, Kenya). *Chem. Geol.* **2012**, *308*, 18–25. [[CrossRef](#)]
2. Dong, N.P.; Yu, Z.B.; Gu, H.H.; Yang, C.G.; Yang, M.X.; Wei, J.H.; Wang, H.; Arnault, J.; Laux, P.; Kunstmann, H. Climate-induced hydrological impact mitigated by a high-density reservoir network in the Poyang Lake Basin. *J. Hydrol.* **2019**, *579*, 124148. [[CrossRef](#)]
3. Xie, J.Q.; You, J.J.; Ma, Z.Z.; Deng, X.Y.; Lin, P.F.; Gao, J.J.; Klemes, J.J. Methodology for including reservoir regulation in water scarcity evaluation. *J. Clean. Prod.* **2022**, *365*, 132657. [[CrossRef](#)]
4. Doretto, A.; Piano, E.; Larson, C.E. The River Continuum Concept: Lessons from the past and perspectives for the future. *Can. J. Fish. Aquat. Sci.* **2020**, *77*, 1853–1864. [[CrossRef](#)]
5. Carey, J.C.; Fulweiler, R.W. Human activities directly alter water-shed dissolved silica fluxes. *Biogeochemistry* **2012**, *111*, 125–138. [[CrossRef](#)]
6. Haojun, D.; Zhen, T.; Quanzhou, G.; Ling, Y.; Yong, F.; Yinhua, L. Research Advance of Changing Biogenic Substance Cycling in River Systems by Damming. *Adv. Earth Sci.* **2018**, *33*, 1237–1247.
7. Vorosmarty, C.J.; Sharma, K.P.; Fekete, B.M.; Copeland, A.H.; Holden, J.; Marble, J.; Lough, J.A. The storage and aging of continental runoff in large reservoir systems of the world. *Ambio* **1997**, *26*, 210–219.
8. Humborg, C.; Conley, D.J.; Rahm, L.; Wulff, F.; Cociasu, A.; Ittekkot, V. Silicon retention in river basins: Far-reaching effects on biogeochemistry and aquatic food webs in coastal marine environments. *AMBIO J. Hum. Environ.* **2000**, *29*, 45–50. [[CrossRef](#)]
9. Ciais, P.; Sabine, C.; Bala, G.; Bopp, L.; Brovkin, V.; Canadell, J.; Thornton, P. Carbon and other biogeochemical cycles. In *Climate Change 2013: The Physical Science Basis; Contribution of Working Group I to the Fifth Assessment Report of the Intergovernmental Panel on Climate Change*; Cambridge University Press: Cambridge, UK, 2014; pp. 46–570.
10. Stocker, T.; Plattner, G.K.; Dahe, Q. *Climate Change 2013: The Physical Science Basis; Contribution of Working Group I to the Fifth Assessment Report of the Intergovernmental Panel on Climate Change* WG1AR5; Intergovernmental Panel on Climate Change (IPCC): Geneva, Switzerland, 2013; pp. 465–570.
11. Temino-Boes, R.; Romero, I.; Paches, M.; Martinez-Guijarro, R.; Romero-Lopez, R. Anthropogenic impact on nitrification dynamics in coastal waters of the Mediterranean sea. *Mar. Pollut. Bull.* **2019**, *145*, 14–22. [[CrossRef](#)]
12. Ivlev, A.A. Global redox cycle of biospheric carbon: Interaction of photosynthesis and earth crust processes. *BioSystems* **2015**, *137*, 1–11. [[CrossRef](#)]
13. Lal, R. Soil erosion and the global carbon budget. *Environ. Int.* **2003**, *29*, 437–450. [[CrossRef](#)] [[PubMed](#)]
14. Hamilton, T.L.; Corman, J.R.; Havig, J.R. Carbon and nitrogen recycling during cyanobacteria in dreissenid-invaded and non-invaded US midwestern lakes and reservoirs. *Hydrobiologia* **2020**, *847*, 939–965. [[CrossRef](#)]
15. Tan, D.B.; Luo, T.F.; Zhao, D.Z.; Li, C. Carbon dioxide emissions from the Geheyan Reservoir over the Qingjiang River Basin, China. *Ecohydrol. Hydrobiol.* **2019**, *19*, 499–514. [[CrossRef](#)]
16. Fuhrmann, B.C.; Beutel, M.W.; O'Day, P.A.; Tran, C.; Funk, A.; Brower, S.; Seelos, M. Effects of mercury, organic carbon, and microbial inhibition on methylmercury cycling at the profundal sediment-water interface of a sulfate-rich hypereutrophic reservoir. *Environ. Pollut.* **2021**, *268*, 115853. [[CrossRef](#)] [[PubMed](#)]
17. Wang, F.; Lang, Y.; Liu, C.Q.; Qin, Y.; Yu, N.; Wang, B. Flux of organic carbon burial and carbon emission from a large reservoir: Implications for the cleanliness assessment of hydropower. *Sci. Bull.* **2019**, *64*, 603–611. [[CrossRef](#)] [[PubMed](#)]
18. Abril, G.; Richard, S.; Guerin, F. In situ measurements of dissolved gases 440 (CO₂ and CH₄) in a wide range of concentrations in a tropical reservoir using an equilibrator. *Sci. Total Environ.* **2006**, *354*, 246–251. [[CrossRef](#)]
19. Phyo, W.W.; Wang, F. A review of carbon sink or source effect on artificial reservoirs. *Int. J. Environ. Sci. Technol.* **2019**, *16*, 2161–2174. [[CrossRef](#)]
20. Han, Q.; Wang, B.; Liu, C.Q.; Wang, F.; Peng, X.; Liu, X.L. Carbon biogeochemical cycle is enhanced by damming in a karst river. *Sci. Total Environ.* **2018**, *616*, 1181–1189. [[CrossRef](#)]
21. Biswas, H.; Mukhopadhyay, S.K.; De, T.K.; Sen, S.; Jana, T.K. Biogenic controls on the air-water carbon dioxide exchange in the Sundarban mangrove environment, northeast coast of Bay of Bengal, India. *Limnol. Oceanogr.* **2004**, *49*, 95–101. [[CrossRef](#)]
22. Hammer, K.J.; Kragh, T.; Sand-Jensen, K. Inorganic carbon promotes photosynthesis, growth, and maximum biomass of phytoplankton in eutrophic water bodies. *Freshw. Biol.* **2019**, *64*, 1956–1970. [[CrossRef](#)]
23. Lash, G.G. Significance of stable carbon isotope trends in carbonate concretions formed in association with anaerobic oxidation of methane (AOM), Middle and Upper Devonian shale succession, western New York State, USA. *Mar. Pet. Geol.* **2018**, *91*, 470–479. [[CrossRef](#)]
24. Kim, S.; Choi, K.; Chung, J. Reduction in carbon dioxide and production of methane by biological reaction in the electronics industry. *Int. J. Hydrogen Energy* **2013**, *38*, 3488–3496. [[CrossRef](#)]

25. Chuang, P.C.; Yang, T.F.; Wallmann, K.; Matsumoto, R.; Hu, C.Y.; Chen, H.W.; Dale, A.W. Carbon isotope exchange during Anaerobic Oxidation of Methane (AOM) in sediments of the northeastern South China Sea. *Geochim. Cosmochim. Acta* **2019**, *246*, 138–155. [[CrossRef](#)]
26. Wang, L.; Xiao, S.B.; Liu, D.F.; Chen, W.Z.; Wang, Y.C.; Chen, X.Y.; Duan, Y.J. Fluxes of greenhouse gases from Xiangxi River in summer and their influencing factors. *Environ. Sci.* **2012**, *33*, 1471–1475.
27. Chanudet, V.; Descloux, S.; Harby, A.; Sundt, H.; Hansen, B.H.; Brakstad, O.; Serça, D.; Guerin, F. Gross CO₂ and CH₄ emissions from the Nam Ngum and Nam Leuk sub-tropical reservoirs in Lao PDR. *Sci. Total Environ.* **2011**, *409*, 5382–5391. [[CrossRef](#)]
28. Wang, W.F.; Li, S.L.; Zhong, J.; Maberly, S.C.; Li, C.; Wang, F.S.; Xiao, H.Y.; Liu, C.Q. Climatic and anthropogenic regulation of carbon transport and transformation in a karst river-reservoir system. *Sci. Total Environ.* **2020**, *707*, 135628. [[CrossRef](#)] [[PubMed](#)]
29. Wang, W.F.; Li, S.L.; Zhong, J.; Wang, L.C.; Yang, H.; Xiao, H.Y.; Liu, C.Q. CO₂ emissions from karst cascade hydropower reservoirs: Mechanisms and reservoir effect. *Environ. Res. Lett.* **2021**, *16*, 044013. [[CrossRef](#)]
30. Pu, J.; Li, J.; Zhang, T.; Martin, J.B.; Yuan, D. Varying thermal structure controls the dynamics of CO₂ emissions from a subtropical reservoir, south China. *Water Res.* **2020**, *178*, 115831. [[CrossRef](#)]
31. Wang, W.; Zhong, J.; Li, C.; Yi, Y.; Chen, S.; Chen, L.; Lang, Y.; Li, S. The influence of cascade reservoir construction on water chemistry distribution in Karst area. *J. Lake Sci.* **2020**, *32*, 713–725.
32. Barros, N.; Cole, J.J.; Tranvik, L.J.; Prairie, Y.T.; Bastviken, D.; Huszar, V.L.; Roland, F. Carbon emission from hydroelectric reservoirs linked to reservoir age and latitude. *Nat. Geosci.* **2011**, *4*, 593–596. [[CrossRef](#)]
33. Zhang, Z.M.; Huang, X.F.; Zhou, Y.C. Spatial heterogeneity of soil organic carbon in a karst region under different land use patterns. *Ecosphere* **2020**, *11*, e03077. [[CrossRef](#)]
34. Cao, M.; Zhou, Z.; Zhang, J.; Zhang, S.; Yin, C.; Yan, L. Study on the physicochemical characteristics and environmental indication of dolomite karst cave water in the Shuanghe Cave, Guizhou Province. *Geochimica* **2017**, *46*, 87–97.
35. Liang, J.; Yi, Y.; Li, X.; Yuan, Y.; Zhai, Y. Detecting changes in water level caused by climate, land cover and dam construction in interconnected riverlake systems. *Sci. Total Environ.* **2021**, *788*, 147692. [[CrossRef](#)] [[PubMed](#)]
36. Invers, O.; Zimmerman, R.C.; Alberte, R.S.; Pérez, M.; Romero, J. Inorganic carbon sources for seagrass photosynthesis: An experimental evaluation of bicarbonate use in species inhabiting temperate waters. *J. Exp. Mar. Biol. Ecol.* **2001**, *265*, 203–217. [[CrossRef](#)]
37. Raymond, P.A.; Hartmann, J.; Lauerwald, R.; Sobek, S.; McDonald, C.; Hoover, M.; Butman, D.; Striegl, R.; Mayorga, E.; Humborg, C.; et al. Global carbon dioxide emissions from inland waters. *Nature* **2013**, *503*, 355–359. [[CrossRef](#)]
38. Myrbo, A.; Shapley, M.D. Seasonal water-column dynamics of dissolved inorganic carbon stable isotopic compositions ($\delta^{13}\text{CDIC}$) in small hardwater lakes in Minnesota and Montana. *Geochim. Cosmochim. Acta* **2006**, *70*, 2699–2714. [[CrossRef](#)]
39. Liu, X. *Study on Geochemical Characteristics of Dissolved Inorganic Carbon in Lakes of Karst Plateau Area: A Case Study in Pingzhai Reservoir*; Guizhou Normal University: Guiyang, China, 2021. [[CrossRef](#)]
40. Chun, H.Z.Y.; Cheng, Z.; Xiaoyu, G.; Chen, W.; Deng, J. Reservoir storage estimation of karst underground reservoir associated with Pingzhai Reservoir in South tributary of Wu River. *Resour. Environ. Eng.* **2021**, *35*, 478–483.
41. Beck, M.B. *Mathematical Modeling of Water Quality*; IASA Working Paper; IASA: Laxenburg, Austria, 1978.
42. Li, J.; Pu, J.; Zhang, T. Transport and transformation of dissolved inorganic carbon in a subtropical groundwater-fed reservoir, south China. *Water Res.* **2022**, *209*, 117905. [[CrossRef](#)]
43. Wang, Y.; Pu, P. Preliminary study on thermocline in Lake Fuxian. *Trans. Oceanol. Limnol.* **1982**, *4*, 1–9.
44. Das, A.; Krishnaswami, S.; Bhattacharya, S.K. Carbon isotope ratio of dissolved inorganic carbon (DIC) in rivers draining the Deccan Traps, India: Sources of DIC and their magnitudes. *Earth Planet. Sci. Lett.* **2005**, *236*, 419–429. [[CrossRef](#)]
45. Helie, J.F.; Hillaire-Marcel, C.; Rondeau, B. Seasonal changes in the sources and fluxes of dissolved inorganic carbon through the St. Lawrence River—Isotopic and chemical constraint. *Chem. Geol.* **2002**, *186*, 117–138. [[CrossRef](#)]
46. Liu, C.Q.; Jiang, Y.K.; Tao, F.X.; Lang, Y.C.; Li, S.L. Chemical weathering of carbonate rocks by sulfuric acid and carbon cycling in Southwest China. *Geochimica* **2008**, *37*, 404–414.
47. Cheng, T.Y.; Zhou, T.; Qin, Y.; Phoye, W.; Wang, F.S. Characters and sources of dissolved inorganic carbon isotope in channel reservoir: A case of Wanan Reservoir. *Chin. J. Ecol.* **2018**, *37*, 661–666.
48. Yang, X.Y.; Li, Y.J.; Wang, B.L.; Xiao, J.; Yang, M.L.; Liu, C.Q. Effect of hydraulic load on thermal stratification in karst cascade hydropower reservoirs, Southwest China. *J. Hydrol. Reg. Stud.* **2020**, *32*, 100748. [[CrossRef](#)]
49. Belolipetskii, V.M.; Genova, S.N. Simplified Mathematical Model of the Hydrothermal Regime of the Krasnoyarsk Reservoir. *Therm. Sci.* **2019**, *23*, S455–S462. [[CrossRef](#)]
50. Qiu, X. *Study on Water Quality Evolution Law and Eutrophication of Stratified Reservoirs in North China*; Xi'an University of Architecture and Technology: Xi'an, China, 2016.
51. Varol, M.; Li, S.Y. Biotic and abiotic controls on CO₂ partial pressure and CO₂ emission in the Tigris River, Turkey. *Chem. Geol.* **2017**, *449*, 182–193. [[CrossRef](#)]
52. Herczeg, A.L. A stable carbon isotope study of dissolved inorganic carbon cycling in a softwater lake. *Biogeochemistry* **1987**, *4*, 231–263. [[CrossRef](#)]
53. Reiss, R.S.; Lemmin, U.; Cimadoribus, A.A.; Barry, D.A. Wintertime Coastal Upwelling in Lake Geneva: An Efficient Transport Process for Deepwater Renewal in a Large, Deep Lake. *J. Geophys. Res.-Ocean.* **2020**, *125*, e2020JC016095. [[CrossRef](#)]

54. Reiss, R.S.; Lemmin, U.; Barry, D.A. Wind-Induced Hypolimnetic Upwelling Between the Multi-Depth Basins of Lake Geneva During Winter: An Overlooked Deepwater Renewal Mechanism? *J. Geophys. Res.-Ocean.* **2022**, *127*, e2021JC018023. [[CrossRef](#)]
55. Wu, Y.; Luo, Z.H.; Luo, W.; Ma, T.; Wang, Y.X. Multiple isotope geochemistry and hydrochemical monitoring of karst water in a rapidly urbanized region. *J. Contam. Hydrol.* **2018**, *218*, 44–58. [[CrossRef](#)]
56. Rao, W.B.; Zheng, F.W.; Tan, H.B.; Yong, B.; Jin, K.; Wang, S.; Zhang, W.B.; Chen, T.Q.; Wang, Y.N. Major ion chemistry of a representative river in South-central China: Runoff effects and controlling mechanisms. *J. Hazard. Mater.* **2019**, *378*, 120755. [[CrossRef](#)]
57. Peng, Y.M.; Xiao, Q.; Xue, H.L.; Lv, M.H.; Lin, G.Q.; Zhao, H.J.; Wu, P.Y.; Guo, Y.L. Comparison of groundwater hydrogeochemistry of karst areas in northern and southern China with emphasis on their performance in karst development. *Carbonates Evaporites* **2022**, *37*, 76.
58. Huang, Q.; Xiaoqun, Q.I.N.; Ruirui, C.H.E.N.G. Research progress of sulfuric acid rain participating in the dissolution of carbonate rocks. *Carsologica Sin.* **2019**, *38*, 149–156.
59. Gaillardet, J.; Dupre, B.; Louvat, P.; Allegre, C.J. Global silicate weathering, Global silicate weathering and CO₂ consumption rates deduced from the chemistry of large rivers. *Chem. Geol.* **1999**, *159*, 3–30. [[CrossRef](#)]

Disclaimer/Publisher’s Note: The statements, opinions and data contained in all publications are solely those of the individual author(s) and contributor(s) and not of MDPI and/or the editor(s). MDPI and/or the editor(s) disclaim responsibility for any injury to people or property resulting from any ideas, methods, instructions or products referred to in the content.